Rapid noise prediction models for serrated leading and trailing edges

Benshuai Lyu[a,*], Lorna J. Ayton[a]

[a] *Department of Applied Mathematics and Theoretical Physics, University of Cambridge, Cambridge CB3 0WA, UK*

Abstract

Leading- and trailing-edge serrations have been widely used to reduce the leading- and trailing-edge noise in applications such as contra-rotating fans and large wind turbines. Recent studies show that these two noise problems can be modelled analytically using the Wiener-Hopf method. However, the resulting models involve infinite-interval integrals that cannot be evaluated analytically, and consequently implementing them poses practical difficulty. This paper develops easily-implementable noise prediction models for flat plates with serrated leading and trailing edges, respectively. By exploiting the fact that high-order modes are cut-off and adjacent modes do not interfere in the far field except at sufficiently high frequencies, an infinite-interval integral involving two infinite sums is approximated by a single straightforward sum. Numerical comparison shows that the resulting models serve as excellent approximations to the original models. Good agreement is also achieved when the leading-edge model predictions are compared with experimental results for sawtooth serrations of various root-to-tip amplitudes, whereas a qualitative evaluation of TE noise model shows that an accurate characterization of the wall pressure statistics beneath turbulent boundary layers is crucial for an accurate TE noise prediction. Importantly, the models developed in this paper can be evaluated robustly in a very efficient manner. For example, a typical far-field noise spectrum can be calculated within milliseconds for both the trailing- and leading-edge noise models on a standard desktop computer. Due to their efficiency and ease of numerical

*Corresponding author
Email address: `bl362@cam.ac.uk` (Benshuai Lyu)

implementation, these models are expected to be of particular importance in applications where a numerical optimization is likely to be needed.

Keywords: aeroacoustics; noise control; scattering

1. Introduction

Aerofoil noise is important in many applications such as contra-rotating fans and large wind turbines. It often involves more than one noise generation mechanism [1, 2]. Of particular relevance are the leading-edge (LE) noise and the turbulent boundary-layer trailing-edge (TE) noise. LE noise is due to the scattering of velocity fluctuations of the incoming flow by the leading-edge of an aerofoil, therefore it is common in applications with multi-row rotors/stators where the wake flow due the front row impinges on the downstream blades/vanes leading to strong flow-structure interactions, such as in jet engines and contra-rotating fans. TE noise, on the other hand, is generated when a (most often) turbulent boundary layer convects past and then gets scattered by the trailing edge of an aerofoil [3]. It is thus common in applications with highly turbulent boundary layers, such as wind turbines.

One of the early research works on LE noise was conducted by Graham [4], where similarity rules were established for the unsteady aerodynamic loading of the aerofoil due to sinusoidal gusts at subsonic speed. Following Graham, Amiet [1] investigated the acoustic response of an aerofoil subject to sinusoidal incoming gusts. Amiet used the Schwarzschild method and related the far-field sound Power Spectral Density (PSD) to the wavenumber spectral density of the incoming velocity fluctuations normal to the aerofoil. With an accurate model for the turbulence wavenumber spectral density, Amiet's approach has been shown to work well and become an important method for following studies.

A serrated LE has been proposed as one of the most promising approaches to reduce LE noise [5, 6, 7, 8, 9], and extensive research has been carried out to study its noise reduction performance and mechanisms. This includes experimental studies such as those by Hansen et al. [8] and Narayanan et al. [9], numerical investigations carried out by Lau et al. [10], Kim et al. [11] and Turner and Kim [12], and analytical examinations such as those by Lyu and

Azarpeyvand [13] and Ayton and Chaitanya [14].

Similarly, TE serrations have been widely used as an effective way of reducing TE noise. A large bulk of literature on this is experimental work. These include studies by Dassen et al. [15], Chong et al. [16], Moreau and Doolan [17], Oerlemans et al. [18], Gruber et al. [19], Chong and Vathylakis [20], Leon et al. [21], etc. Numerical techniques have also been widely used to study the TE serrations as a way of reducing TE noise, see for example those by Jones and Sandberg [22], Sanjosé et al. [23] and van der Velden et al. [24]. A number of authors have also conducted analytical studies. Some of the early analytical works include those by Howe [25, 26], where a tailored Green's function was used to predict the far-field sound generated by flat plates with sinusoidal and sawtooth serrations, respectively. However, Howe's model dramatically overpredicted the sound reduction achieved by using TE serrations. Howe's approach was later used by Azarpeyvand et al. [27] to study the noise reduction characteristics of other serration geometries. The recent work by Lyu et al. [28, 29], on the other hand, used Amiet's approach and extended Amiet's model [30, 31] for a straight trailing edge to the serrated case. The results showed that the principal noise reduction mechanism was due to the destructive interference and the predicted noise reduction was more realistic compared to experimental results.

Although the TE noise and LE noise are due to different noise generation mechanisms, mathematically they bear a striking similarity, hence, the techniques used to model the two problems are expected to be similar to each other. For example, recent work [32, 14] shows that both the serrated LE noise and TE noise can be modelled analytically using the Wiener-Hopf method. This approach has shown good agreement with experiments for LE noise [14]. However, both the LE and TE solutions involve an infinite-interval integral and two sums over infinitely many scattering modes, which make their implementations both difficult and error-prone.

The issue is addressed in this paper. By exploiting the fact that high-order modes are cut-off and little coupling between expanded modes occurs except at very high frequencies, we replace the infinite-interval integral that involves two infinite sums with one straightforward sum. The simplified model takes a particularly concise form when the serration wavelength is small compared to the transformed acoustic wavelength. The final results can therefore be easily implemented numerically in a robust and efficient manner.

This paper is structured as follows. Section 2 shows the essential analytical steps to reach the final results for both the LE and TE noise problems, respectively. Section 3 presents a comparison between the approximated results obtained in this paper and those obtained from the full analytical solutions. The following section uses the simplified leading-edge model to compare with the leading-edge noise spectra observed in experiments. The final section concludes this paper and lists directions for future work.

2. The leading-edge and trailing-edge noise models

As mentioned in Section 1, the TE and LE noise problems bear a striking similarity between each other. In either case, to allow the analytical derivation to continue, the serrated aerofoil is often assumed to be a semi-infinite plate [1, 33, 14, 13, 28] placed in a uniform incoming flow of constant density $\tilde{\rho}$ and velocity $\tilde{U}$ at zero angle of attack, as shown in figure 1. The speed of sound is denoted by $\tilde{c}_0$. In the rest of this paper, the serration wavelength is used to normalized the length dimension, while $\tilde{\rho}$ and $\tilde{U}$ are used to non-dimensionalize other dynamic variables such as the velocity potential and pressure. In this paper, we restrict our attention to periodic leading-edge and trailing-edge serrations. Because the geometric parameters are normalized by the serration wavelength, the serrations have a period 1. The normalized root-to-tip length is given by $2h$. Let x, y, z denote the streamwise, spanwise and normal to the plate directions, respectively, and the coordinate origin is fixed in the middle between the root and tip. In such a coordinate frame, the serration profile can be described by $x = hF(y)$, where $F(y)$ is a single-valued function that has a maximum value 1 and minimum value -1. Moreover, we require 1 to be the smallest period. Other than these constraints, the function $F(y)$ is arbitrary.

Figure 1 illustrates the geometric similarity and coordinate symmetry of the leading-edge and trailing-edge configurations. Despite this symmetry, the physics they represent is quite different. For the leading-edge problem, the unsteady flow fluctuations, due to the incoming turbulence convected by the

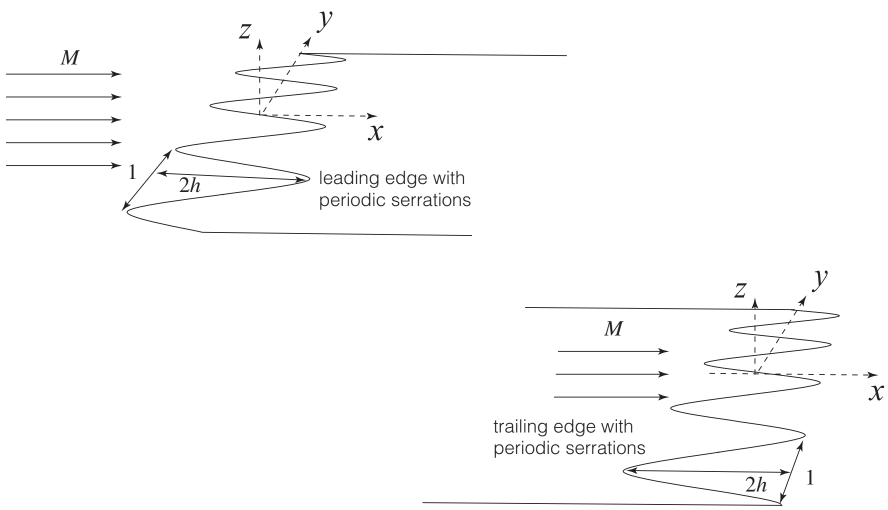

Figure 1: Schematic illustrations of the simplified semi-infinite flat plate with leading-edge and trailing-edge serrations. Both the trailing-edge and leading-edge serrations are periodic and have a non-dimensional wavelength of 1 and root-to-tip amplitude of $2h$. Uniform flows of Mach number M are shown in both configurations, which bear a striking geometric similarity due to coordinate symmetry.

mean flow, are scattered into sound near the leading edge of the flat plate, whereas in the trailing-edge problem the source of scattering is the turbulence beneath turbulent boundary layers. The boundary conditions required by these two problems are therefore quite different. As such, we need to discuss them separately.

2.1. The leading-edge noise problem

When the turbulence in the mean flow passes the leading edge, a scattered potential flow is induced. The scattered potential ensures that appropriate boundary conditions are satisfied. In the leading-edge noise problem, the vertical velocity fluctuation of the incoming turbulence is of primary concern. The turbulence in the mean flow consists of a wide range of time and length scales. However, one can always perform a Fourier Transformation on the incoming vertical velocity field, such that it can be written as

$$w_i = \int_{-\infty}^{\infty} \hat{w}_0(\omega, k_2)\mathrm{e}^{\mathrm{i}(-\omega t + k_1 x + k_2 y)}\mathrm{d}k_2, \tag{1}$$

where t denotes time, $\hat{w}_0$ the velocity fluctuation in the z direction, ω the angular frequency and k_1 and k_2 the wavenumbers in the streamwise and spanwise directions, respectively. The turbulence is assumed to be frozen and convects downstream at a non-dimensional speed of 1. Therefore, one has $k_1 = \omega$.

Let ϕ_s denote this scattered velocity potential. One can show that ϕ_s satisfies the convective wave equation

$$\nabla^2 \phi_s - M^2 \left(\frac{\partial}{\partial t} + \frac{\partial}{\partial x} \right)^2 \phi_s = 0, \tag{2}$$

where $M = \tilde{U}/\tilde{c}_0$. To ensure that the normal velocity on the plate vanishes, we require

$$\left. \frac{\partial \phi_s}{\partial z} \right|_{z=0} = -w_i, \quad x > hF(y). \tag{3}$$

The scattering problem is anti-symmetric across $z = 0$, therefore we also have

$$\phi_s|_{z=0} = 0, \quad x < hF(y). \tag{4}$$

This mixed boundary condition problem can be solved using the Wiener-Hopf method [14, 34]. For the sake of brevity we omit the details of the solving procedure. Interested readers are referred to Ayton and Chaitanya [14] and the appendix of Lyu et al. [34]. Here we only give the results in the acoustical far-field as

$$p(\omega, r, \theta, y) \approx \int_{-\infty}^{\infty} H_l(\omega, \boldsymbol{x}, k_2) \hat{w}_0(\omega, k_2) \mathrm{d}k_2, \tag{5}$$

where

$$H_l(\omega, \boldsymbol{x}, k_2) = \frac{\mathrm{e}^{\mathrm{i}\pi/4}}{\sqrt{\pi}} \mathrm{e}^{-\mathrm{i}kMx/\beta^2} \cos\frac{\theta}{2} \sum_{n=-\infty}^{\infty} \frac{k_1/\beta^2 - \kappa_n \cos\theta}{\bar{k}_1 - \kappa_n \cos\theta} \frac{1}{\sqrt{\bar{k}_1 + \kappa_n}} \frac{\mathrm{e}^{\mathrm{i}\kappa_n r}}{\sqrt{r}} \mathrm{e}^{\mathrm{i}\chi_n y} E_n(-\kappa_n \cos\theta). \tag{6}$$

In equation 6, r, θ and y denote, respectively, the radial, polar and axial axes of the stretched cylindrical coordinate system $(x/\beta, y, z)$, i.e. y denotes the axial axis and θ is the polar angle to the stretched axis x/β in the $(x/\beta, z)$ plane ($\theta = 0$ corresponds to the x/β axis) and $r = \sqrt{(x/\beta)^2 + z^2}$. In addition, one has $k = \omega M$, $\beta = \sqrt{1 - M^2}$, $\bar{k}_1 = k_1/\beta$, $\chi_n = k_2 + 2n\pi$, $\kappa_n = \sqrt{k^2 - \chi_n^2}$ and

$$E_n(-\kappa_n \cos\theta) = \int_0^1 \mathrm{e}^{\mathrm{i}(\bar{k}_1 - \kappa_n \cos\theta)\bar{h}F(\eta)} \mathrm{e}^{-\mathrm{i}2n\pi\eta} \mathrm{d}\eta, \tag{7}$$

where $\bar{h} = h/\beta$.

Since the incoming turbulence is statistically stationary, the far-field sound is best formulated statistically. Routine procedure shows that the far-field sound PSD is given by

$$\Psi(\omega, r, \theta, y) = \lim_{T\to\infty} \frac{\pi}{T} p(\omega, r, \theta, y) p^*(\omega, r, \theta, y), \tag{8}$$

where $2T$ is the time interval used to performed temporal Fourier transform to obtain p and the asterisk denotes the complex conjugate. Substituting equation 5 into 8, we can show that

$$\begin{aligned}\Psi(\omega, r, \theta, y) \approx &\frac{1}{\pi r} \cos^2 \frac{\theta}{2} \\ &\times \int_{-\infty}^{\infty} \Pi_l(\omega, k_2) \sum_{n=-\infty}^{\infty} \frac{k_1/\beta^2 - \kappa_n \cos\theta}{\bar{k}_1 - \kappa_n \cos\theta} \frac{E_n(-\kappa_n \cos\theta)}{\sqrt{\bar{k}_1 + \kappa_n}} \mathrm{e}^{\mathrm{i}\chi_n y} \mathrm{e}^{\mathrm{i}\kappa_n r} \\ &\times \sum_{m=-\infty}^{\infty} \left[\frac{k_1/\beta^2 - \kappa_m \cos\theta}{\bar{k}_1 - \kappa_m \cos\theta} \frac{E_m(-\kappa_m \cos\theta)}{\sqrt{\bar{k}_1 + \kappa_m}} \mathrm{e}^{\mathrm{i}\chi_m y} \mathrm{e}^{\mathrm{i}\kappa_m r} \right]^* \mathrm{d}k_2,\end{aligned} \tag{9}$$

where $\Pi_l(\omega, k_2)$ is the wavenumber frequency spectrum of the vertical velocity fluctuations due to the incoming turbulence.

Experiments and theories have shown that narrow serrations (a small serration wavelength) are more effective than wide serrations in reducing the LE noise [9, 13]. This is related to the spanwise correlation length of the incoming gust, hence to the integral scale of the incoming turbulence. A detailed discussion was given by Lyu and Azarpeyvand [13] and Lyu et al. [34]. Consequently, for practical usage, we only need to restrict our attention to narrow serrations. Under the assumption of narrow serrations, equation 9 can be further simplified. First, we only need to investigate the case where both κ_n and κ_m are real, because otherwise the exponential term $\mathrm{e}^{\mathrm{i}\kappa_n r}(\mathrm{e}^{\mathrm{i}\kappa_m r})^*$ causes the whole term to decay exponentially in the far field. Noting that $\kappa_n = \sqrt{\bar{k}^2 - \chi_n^2}$, we see that κ_n is real only when $-\bar{k} < \chi_n < \bar{k}$. Because we restrict to the case where the serration wavelength is small, in the frequency range of interest we may have the convective acoustic wavenumber $\bar{k} < \pi$. It is, therefore, permissible to have

$$\mathrm{e}^{\mathrm{i}\kappa_n r}(\mathrm{e}^{\mathrm{i}\kappa_m r})^* = \delta_{nm} \mathrm{sgn}(\Re(\kappa_n)), \tag{10}$$

where $\mathrm{sgn}(0) = 0$ and $\mathrm{sgn}(x) = \pm 1$ when $\pm x > 0$. Note equation 10 shows that its right-hand side vanishes when κ_n is imaginary. This implies that

$$\Psi(r,\theta,y) \sim \frac{1}{\pi r}\cos^2\frac{\theta}{2}\sum_{n=-\infty}^{\infty}\int_{-\infty}^{\infty}\Pi_l(\omega,k_2) \times \left|(k_1/\beta^2-\kappa_n\cos\theta)\frac{E_n(-\kappa_n\cos\theta)}{(-\kappa_n\cos\theta+\bar{k}_1)\sqrt{\bar{k}_1+\kappa_n}}\right|^2 \mathrm{sgn}(\Re(\kappa_n))\mathrm{d}k_2. \tag{11}$$

Second, in light of the fact that κ_n is real only when $-\bar{k} < \chi_n < \bar{k}$ and the serration wavelength is small, the integrand does not vanish only when $-2n\pi - \bar{k} \leq k_2 \leq -2n\pi + \bar{k}$. Over such a typically small range of k_2, the integrand of equation 5 does not vary significantly due to its algebraic dependence on k_2 (provided the Mach number is not close to 1). Hence we can take the k_2 dependence out of the integral, and change the integration interval to $-2n\pi - \bar{k}$ to $-2n\pi + \bar{k}$, without causing significant errors. Upon doing so, equation 5 simplifies to

$$\Psi(r,\theta,y) \sim \frac{2\bar{k}}{\pi r}\cos^2\frac{\theta}{2}\frac{(k_1/\beta^2-\bar{k}\cos\theta)^2}{(\bar{k}_1-\bar{k}\cos\theta)^2(\bar{k}_1+\bar{k})}\sum_{n=-\infty}^{\infty}\Pi_l(\omega,2n\pi)\left|E_n(-\bar{k}\cos\theta)\right|^2. \tag{12}$$

Equation 12 is of a remarkably neat form compared to the original solution given by Ayton and Chaitanya [14]. The infinite-interval integral over k_2 and one of the two infinite sums have been eliminated, and the final solution is shown as a simple sum. This not only permits a rapid numerical evaluation, but also facilitates the use of wavenumber frequency spectra of the vertical velocity fluctuations obtained directly from numerical and experimental data. Moreover, equation 12 is uniformly valid as a far-field solution for the entire frequency range irrespective of the value of r, whereas the original solution in Ayton and Chaitanya [14] exhibits convergence problems at low frequencies because the choice of r also depends on frequency.

Equation 12 is obtained by assuming that the serrations are narrow. It would of course be useful to know how narrow can be regarded as appropriate. This can be obtained from the criterion that the convective acoustic wavenumber $\bar{k} < \pi$ (recall that lengths are non-dimensionlised by the serration wavelength). In fact, when $\pi < \bar{k} \leq 2\pi$, the overlap between adjacent modes is still rather weak, therefore it is often permissible to assume that the approximation is still valid when $\bar{k} \leq 2\pi$. It is clear that this inequality depends only on the (dimensional) serration wavelength, (dimensional) acoustic wavenumber and Mach number. This is likely to be satisfied in practical applications. To put this into perspective, let us take a typical example applicable in the wind industry for an aerofoil of chord 1 m placed in a mean flow of Mach number 0.2. The serration wavelength is around 2 cm while the serration root-to-tip is around 10 cm. The inequality will therefore hold for a frequency up to 17 KHz, which is near the upper limit of the audible frequency range. Thus, our approximation is valid for the full range of practical interest in this case.

2.2. The trailing-edge noise problem

When the turbulent boundary layer convects past the trailing edge of a flat plate, a scattered pressure field is induced. In a similar manner, we may write the wavenumber frequency spectrum of the wall pressure fluctuations beneath the boundary layer as

$$p_i = \int_{-\infty}^{\infty} \hat{p}_0(\omega, k_2) \mathrm{e}^{\mathrm{i}(-\omega t + k_1 x + k_2 y)} \mathrm{d}k_2, \tag{13}$$

where relevant quantities are defined in a similar way as those defined in section 2.1, except here $\hat{p}_0$ is the amplitude of the Fourier component of wall pressure fluctuations and $k_1 = \omega/\alpha$, where α is a constant. In other words, these pressure fluctuations are assumed to convect at a speed of α. Here we use a typical value of $\alpha \approx 0.7$ [28].

Let p_s denote the scattered pressure field, which satisfies the convective wave equation, i.e.

$$\nabla^2 p_s - M^2 \left(\frac{\partial}{\partial t} + \frac{\partial}{\partial x} \right)^2 p_s = 0. \tag{14}$$

The boundary conditions are such that the normal velocity on the plate vanishes, i.e.

$$\left. \frac{\partial p_s}{\partial z} \right|_{z=0} = 0, \quad x < hF(y), \tag{15}$$

and that the scattered pressure is 0 on the semi-infinite plane $z = 0$ and $x > hF(y)$, i.e.

$$\Delta p_s|_{z=0} = -p_i, \quad x > hF(y), \tag{16}$$

where Δp_s denotes the pressure jump across the plate. The solution p_s satisfying equation 2 subject to the boundary conditions shown in equations 15 and 16 can be found (see for example Ayton [32]) to be

$$p_s(\omega, r, \theta, y) \approx \int_{-\infty}^{\infty} H_t(\omega, \boldsymbol{x}, k_2)\hat{p}_0(\omega, k_2)\mathrm{d}k_2, \tag{17}$$

where

$$\begin{aligned} H_t(\omega, \boldsymbol{x}, k_2) = {} & \frac{\mathrm{e}^{\mathrm{i}\pi/4}}{\sqrt{\pi}} \mathrm{e}^{-\mathrm{i}kMx/\beta^2} \sin\frac{\theta}{2} \\ & \times \sum_{n=-\infty}^{\infty} \frac{\sqrt{-\bar{k}_1 - \kappa_n}}{2\mathrm{i}(\bar{k}_1 - \kappa_n \cos\theta)} \frac{\mathrm{e}^{\mathrm{i}\kappa_n r}}{\sqrt{r}} \mathrm{e}^{\mathrm{i}\chi_n y} E_n(-\kappa_n \cos\theta), \end{aligned} \tag{18}$$

where r, θ are defined similar to those shown in Section 2.1. In addition, χ_n and κ_n are defined the same as those in Section 2.1. However, we now define $\bar{k}_1 = (k_1 + (kM - k_1M^2))/\beta$ and

$$E_n(-\kappa_n \cos\theta) = \int_0^1 \mathrm{e}^{\mathrm{i}(\bar{k}_1 - \kappa_n \cos\theta)\bar{h}F(\eta)} \mathrm{e}^{-\mathrm{i}2n\pi\eta}\mathrm{d}\eta, \tag{19}$$

where $\bar{h}$ is similarly defined as h/β. Note here that the definitions of k_1 and $\bar{k}_1$ in this trailing-edge noise problem are different from those in the leading-edge noise problem.

In a very similar manner, the far-field sound PSD can be approximated, upon assuming the serration wavelength is sufficiently small such that $\bar{k} < \pi$, to be

$$\begin{aligned} \Psi(r, \theta, y) \sim {} & \frac{1}{4\pi r} \sin^2\frac{\theta}{2} \\ & \times \sum_{n=-\infty}^{\infty} \int_{-\infty}^{\infty} \Pi_t(\omega, k_2) \left| \frac{\sqrt{-\bar{k}_1 - \kappa_n}}{(\bar{k}_1 - \kappa_n \cos\theta)} E_n(-\kappa_n \cos\theta) \right|^2 \mathrm{sgn}(\Re(\kappa_n))\mathrm{d}k_2, \end{aligned} \tag{20}$$

where $\Pi_t(\omega, k_2)$ denotes the wall pressure fluctuations wavenumber frequency spectrum beneath the turbulent boundary layer close to the trailing edge. Equation 20 can be further simplified by replacing the integral with a simple sum to be

$$\Psi(r, \theta, y) \sim \frac{\bar{k}}{2\pi r} \sin^2\frac{\theta}{2} \frac{\bar{k}_1 + \bar{k}}{(\bar{k}_1 - \bar{k}\cos\theta)^2} \sum_{n=-\infty}^{\infty} \Pi_t(\omega, 2n\pi) \left| E_n(-\bar{k}\cos\theta) \right|^2. \tag{21}$$

Similar to equation 12, equation 21 is of a particularly neat form and uniformly valid irrespective of the value of r, and it permits both rapid numerical implementation and the use of numerical or experimental wall pressure statistics as input. It is worth noting equation 21 bears a striking similarity to equation 2.59 in the work of Lyu et al. [28]. The fact that two completely different approaches lead to consistent results of the same form shows that the essential physics are captured in both models. These two equations both show that higher-order modes are still cut-on and contribute to the far-field, therefore the earlier argument in Ayton [32] that higher-order modes were neglected in the model of Lyu et al. [28] was erroneous.

3. Comparison with exact solutions

In Section 2, we reduce the complex original model to a straightforward sum and simplify the result significantly when the serrations are sufficiently narrow (i.e. serration wavelength is small compared to the transformed acoustic wavelength). In this section, to assess how accurate the approximations are, we perform a direction comparison between the full and the simplified solutions. Firstly, we choose to compare the solutions for LE serrations of a sawtooth profile as an illustration.

3.1. The leading-edge noise problem

To enable this comparison, we need a realistic wavenumber spectrum $\Pi_l(\omega, k_2)$ to model the incoming turbulence. There are a number of empirical models available and the LE noise prediction model does not depend on any specific spectral models. As an illustration, here we use the one developed from Von Kármàn spectrum. Based on this, it can be shown that $\Pi_l(\omega, k_2)$, i.e. the wavenumber frequency spectrum of the oncoming normal fluctuation velocity, can be written as [1, 35, 13]

$$\Pi_l(\omega, k_2) = \frac{4\mathrm{TI}^2}{9\pi k_e^2}\frac{\hat{k}_1^2+\hat{k}_2^2}{(1+\hat{k}_1^2+\hat{k}_2^2)^{7/3}}, \tag{22}$$

where TI denotes the turbulent intensity and k_e, $\hat{k}_1$ and $\hat{k}_2$ are given by

$$k_e = \frac{\sqrt{\pi}\Gamma(5/6)}{L_t\Gamma(1/3)}, \quad \hat{k}_1 = \frac{k_1}{k_e}, \quad \hat{k}_2 = \frac{k_2}{k_e}. \tag{23}$$

In the above equations, L_t is the integral scale of the turbulence (also normalized by the serration wavelength) and $\Gamma(x)$ is the Gamma function.

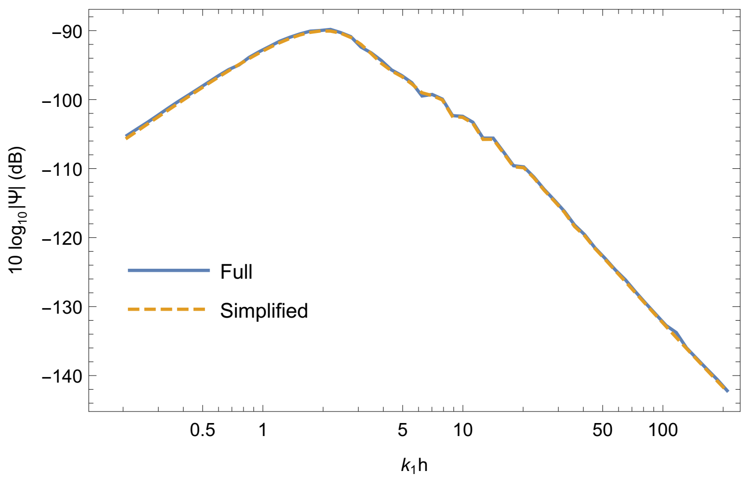

Figure 2: Comparison of predicted LE noise spectra from the full and simplified models: $M = 0.18$, $\mathrm{TI} = 0.025$, $h = 5$, $L_t = 0.3$, $r = 30$, $\theta = 90°$ and $y = 0$.

In order to put equation 22 into perspective, we require a realistic set of physical parameters of the incoming flow. For the sake of convenience, we use those given in previous experiments [9, 13], where $M = 0.18$, $\mathrm{TI} = 0.025$ and $L_t = 0.3$. As an illustrative example, we use sawtooth serrations with $h = 5$. The observer distance is fixed at $r = 30$ in the plane of $y = 0$, but the observer angle is varied from $\theta = 90°$ to $20°$. The far-field PSDs are evaluated from equations 9 and 12, respectively.

The comparison of the predicted noise spectra at $\theta = 90°$ is shown in figure 2. The solid line is obtained from the full solution, i.e. equation 9, while the dashed line is from the simplified solution, i.e. equation 12. It is clear that the two solutions agree excellently over the entire frequency range of interest. We choose $h = 5$ because this represents sharp serrations where the approximation is the least accurate. At such a large value of h we can hardly see the difference between the full and simplified solutions. We can therefore expect at least similar, if not better, agreement for smaller values of h.

Figure 2 is for a fixed observer at 90° above the leading edge. Figure 3 shows the predicted noise spectra for the observer at $\theta = 45°$. The agreement is similar to that shown in figure 2, and the simplified model serves as an excellent approximation to the fully integrated solution. Figure 4 shows the simplified

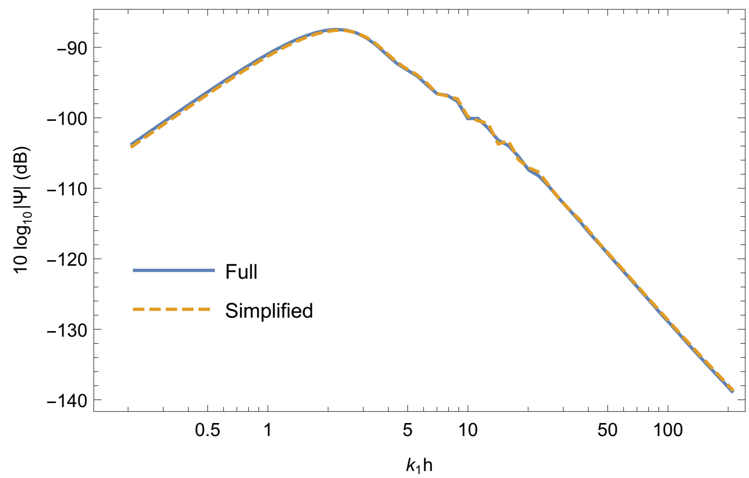

Figure 3: Comparison of predicted LE noise spectra from the full and simplified models: $M = 0.18$, $\mathrm{TI} = 0.025$, $h = 5$, $L_t = 0.3$, $r = 30$, $\theta = 45°$ and $y = 0$.

and full spectra when $\theta = 20°$, and the agreement continues to be very good.

It is worth mentioning, however, the computational costs are very different for the two solutions. For the full integral solution given by equation 9, it takes around one hour and a half to obtain the noise spectrum at a single observer location, whereas on average only 5 ms is needed for the simplified model given by equation 12. The simplified model is faster than the original model by a factor of around $720,000$. More importantly, since no numerical integration of irregular integrands is involved, the computation is much more robust.

3.2. The trailing-edge noise problem

We now compare the approximated model to the full model for the TE noise problem. Similarly, the wall pressure wavenumber spectrum needs to be modelled. As an illustrative example, it suffices to choose Chase's model [36, 28], i.e.

$$\Pi_t(\omega, k_2) = \frac{4C_m v^{*4}\delta^4 k_1^2}{\alpha\left[(k_1^2 + k_2^2)\delta^2 + \chi^2\right]^2}, \tag{24}$$

where $C_m \approx 0.1533$, $v^* \approx 0.03$, $\chi \approx 1.33$, and δ denotes the non-dimensional boundary layer thickness. In this paper, we let δ take an approximate value of 1.01, which corresponds to a realistic non-dimensional boundary layer thickness for a dimensional chord length of 1 m when the serration wavelength is 0.02 m.

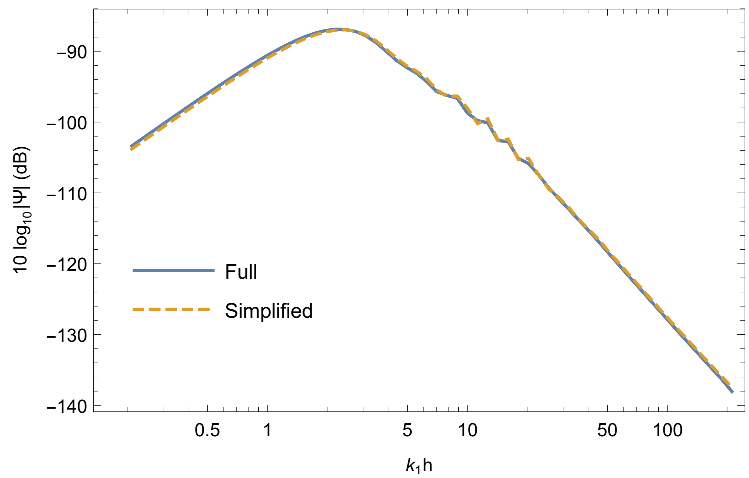

Figure 4: Comparison of predicted LE noise spectra from the full and simplified models: $M = 0.18$, $\mathrm{TI} = 0.025$, $h = 5$, $L_t = 0.3$, $r = 30$, $\theta = 20°$ and $y = 0$.

To enable a direct comparison between the approximated and full results, we again use a sawtooth serration profile with $h = 5$. The observer distance is fixed to be $r = 30$ in the plane of $y = 0$, and the observer angle is varied from $\theta = 90°$ to $20°$. The predicted far-field spectra are plotted using the full solution based on equation 17 and the approximated solution shown in equation 21, respectively.

The comparison of the noise spectra at $\theta = 90°$ is shown in figure 5. As we can see the approximated solution agrees with the full solution with virtually no difference over the entire frequency range. Note that when $k_1 h$ is close to 500, $\bar{k}$ is slightly larger than 2π. But the difference between the two lines is still hardly observable. Therefore, the condition $\bar{k} < 2\pi$, although likely to be satisfied in most practical cases, may be further relaxed in practice.

Figure 5 shows the comparison of the predicted spectra for $\theta = 45°$. The agreement continues to be very good, except slight disagreement occurring near the minima of the oscillation frequencies. The strong oscillations predicted by the models are due to the large value of h, i.e. the use of sharp serrations, leading to strong destructive interference (in experiments, however, these large dips are unlikely to be observed since the turbulence within the boundary layer is not strictly frozen). We choose this large value to examine how the simplified model works in the least accurate case. Had we used smaller values of h, these

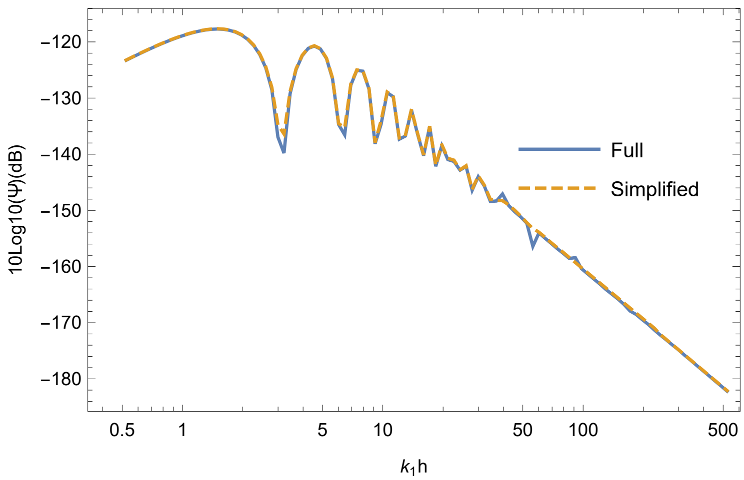

Figure 5: Comparison of predicted TE noise spectra from the full and simplified models: $M = 0.1$, $h = 5$, $\delta = 1.01$, $r = 30$, $\theta = 90^{\circ}$ and $y = 0$.

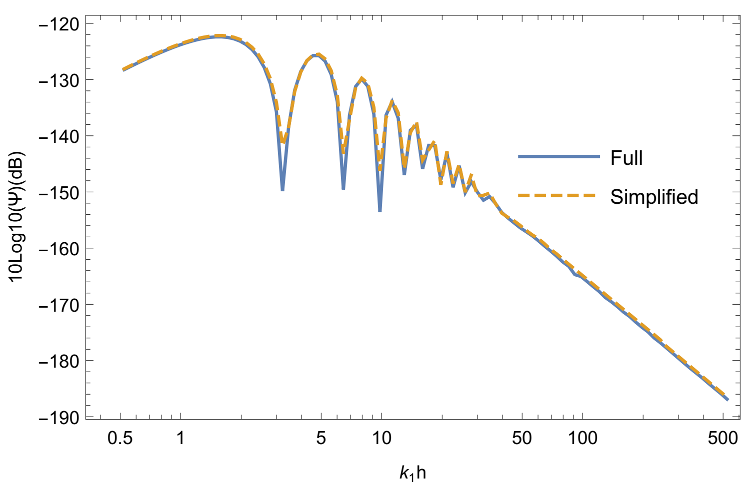

Figure 6: Comparison of predicted TE noise spectra from the full and simplified models: $M = 0.1$, $h = 5$, $\delta = 1.01$, $r = 30$, $\theta = 45^{\circ}$ and $y = 0$.

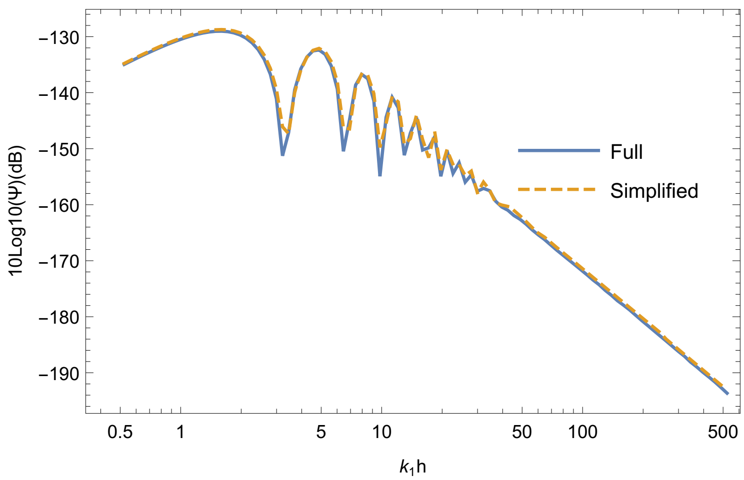

Figure 7: Comparison of predicted TE noise spectra from the full and simplified models: $M = 0.1$, $h = 5$, $\delta = 1.01$, $r = 30$, $\theta = 20°$ and $y = 0$.

oscillations would have disappeared [32].

Figure 7 shows the two predicted spectra when $\theta = 20°$. The agreement continues to be very good over the entire frequency range of interest. Although the two spectra are virtually identical, the computational costs in obtaining them are, as those observed in the LE noise problem, strikingly different: while the full solution demands an hour for computing a single spectrum, the simplified model on average only needs a few milliseconds. In summary, the approximated solution serves as an efficient model for the TE noise problem. More importantly, the simplified TE noise model can be easily implemented and the computation is very robust, while the numerical integration in the full solution is prone to error due to the non-smooth behaviour of the integrand.

4. Comparison with experiments

Results from these simplified models can be directly compared with experimental data. Due to the similar nature of approximation, it suffices to focus on the leading-edge model. Nevertheless, for completeness we also include some experimental results on TE noise subsequently. For the LE model, we choose to compare with the recent experimental results reported in Ayton and Chaitanya

[14] and use the sawtooth serration as an example.

4.1. Leading-edge noise

The experiment was carried out in the acoustic wind tunnel at the Institute of Sound and Vibration of Southampton University. The test facility features a 8 m $\times$ 8 m $\times$ 8 m anechoic chamber and a low-speed wind tunnel with a nozzle of 150 mm $\times$ 450 mm. More details on the test facility can be found in Ayton and Chaitanya [14]. Flat plates having a chord of 150 mm and span of 450 mm with serrated leading edges were placed in the middle of the rectangular jet such that the mean LE line was 150 mm downstream of the nozzle exit. The serrations had a wavelength of 25 mm, but the half root-to-tip amplitude was varied from 6.25 mm to 25 mm. Therefore, the corresponding h was varied from 1/4 and 1.

Free stream turbulence was generated by a rectangular grid of 630 mm $\times$ 690 mm inside the contraction section located 75 cm upstream from the nozzle exit. The dimensionless turbulence spectrum $\Pi_l(\omega, k_2)$ was characterised using the Liepmann model, i.e.

$$\Pi_l(\omega, k_2) = \frac{3\mathrm{TI}^2 L_t^2}{4\pi} \frac{L_t^2(k_1^2 + k_2^2)}{(1 + L_t^2(k_1^2 + k_2^2))^{5/2}}, \tag{25}$$

where TI and L_t were, as defined in section 3.1, the turbulence intensity and streamwise integral length scale, respectively. Note that we use Liepmann model here partly because it was used by Ayton and Chaitanya [14] and we wish to be consistent with the earlier result, and partly because we wish to demonstrate that the noise prediction model does not depend on any specific spectral models for the incoming turbulence and changing it is very straightforward due to the simple nature of equation 12. In fact, the remarkably simple form of equation 12 directly facilitates the use of numerical or experimental turbulence spectra in predicting LE noise. With equation 25, equation 12 can be quickly evaluated and the results can be compared with the noise spectra obtained in the experiment. These are presented in figures 8 to 10, where not only the absolute LE noise spectra but also the noise reduction spectra are shown. To have an intuitive understanding of the frequency and amplitude, noise spectra are shown in their dimensional forms.

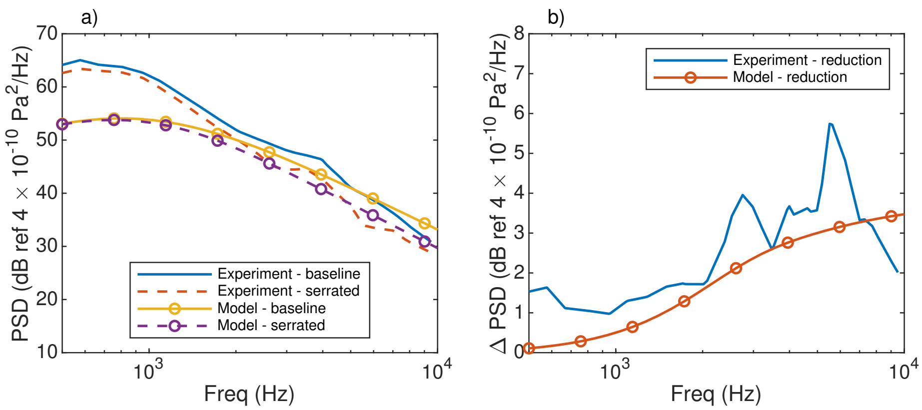

Figure 8: Comparison of the noise spectra between model prediction and experimental measurements when $h = 1/4$.

We start comparing the model and experimental results for the short serration, i.e. for $h = 1/4$. The far-field noise spectra are presented in figure 8(a). Both the serrated and baseline ($h = 0$) spectra are shown. It is well known that in leading-edge noise experiments the low-frequency sound measured in the far field is dominated by jet noise. Therefore, we do not make a direct comparison for frequencies less than 2000 Hz. Good agreement is achieved, however, in the frequency range of 2000 to 10000 Hz for the baseline spectra. This shows that the simplified model works well for straight edges. In addition, the model predicts that a noise reduction of around 3 dB can be achieved by using the short serration of $h = 1/4$, as shown in figure 8(b). The experimental data agree with such a prediction very well.

Figure 9 shows the comparison for $h = 1/2$. As can be seen from figure 9(a), using the longer serration results in a higher noise reduction of up to 8 dB in the experiment. The model can capture this change accurately and the resulting spectrum for the serrated edge agrees very well with that observed in the experiment. This is not surprising given that the simplified model agrees with the full solution to a high degree of accuracy. From the noise reduction spectra, shown in figure 9(b), one can see that at the very high frequencies, the observed noise reduction starts to drop. This signifies the emerging influence of other noise sources, such as TE noise, the effect of which will be more evident

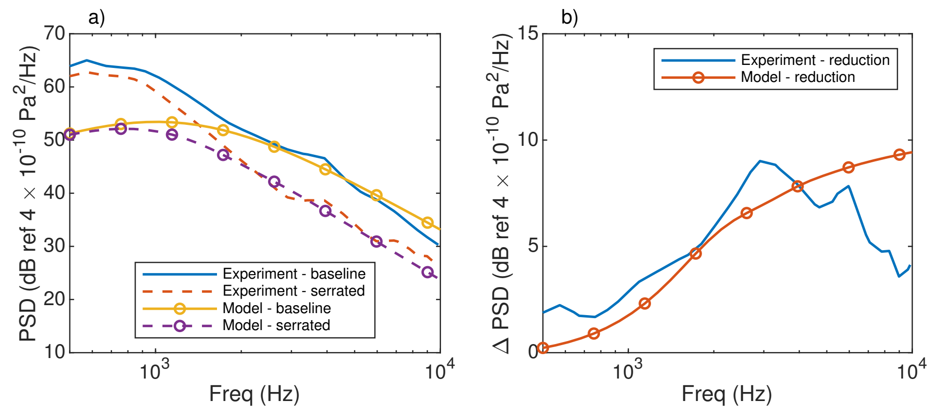

Figure 9: Comparison of the noise spectra between model prediction and experimental measurements when $h = 1/2$.

in the following figure.

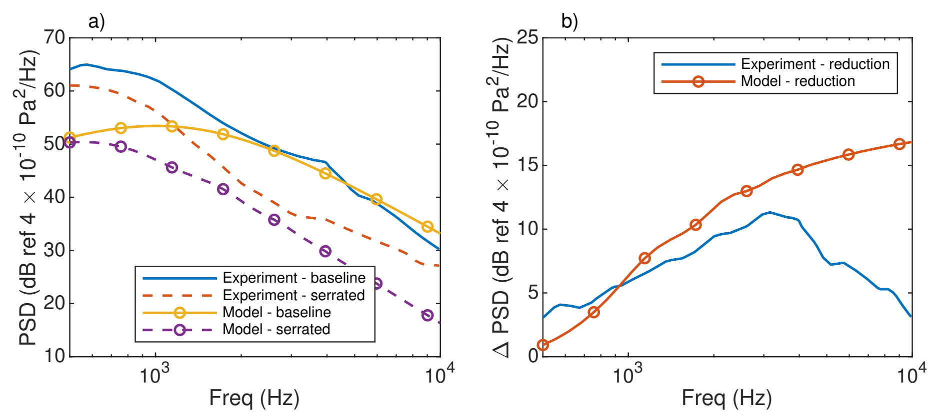

Figure 10: Comparison of the noise spectra between model prediction and experimental measurements when $h = 1$.

Figure 10 shows the comparison for the long serration, i.e. for $h = 1$. We expect an even greater noise reduction due to the use of serrations, and this is confirmed by the experiment, which shows a noise reduction of up to more than 10 dB, as shown in figure 10(a). However, the predicted noise reduction is around 15 dB. The model therefore underpredicts the noise emitted by flat plates with long leading-edge serrations, especially at high frequencies, as shown in figure 10(b). However, this is not due to the failure of the simplified model, but rather due to the effect of neglecting the contribution of trailing-edge noise, which occurs in the experiment and begins to dominate when leading-edge noise is sufficiently suppressed. In their recent work, Bampanis et al. [37] used source localization techniques to filter out TE noise, and they found that once TE noise is removed, LE noise reduction continues to increase as frequency increases, and a noise reduction of more than 15 dB can be observed. This is consistent with our current prediction, as can be seen from figure 10(b). Moreover, it has been shown by Ayton and Chaitanya [14] that adding in a trailing-edge noise contribution results in good agreement with the experimental spectrum. However, as this section is aimed at verifying the LE noise model, the trailing-edge noise contribution has been excluded.

Figures 8 and 10 show that the simplified model serves as an accurate approximation to the full solution, which is both computationally expensive and error-prone. The simplified model overcomes these two issues and is both efficient and robust.

4.2. Trailing-edge noise

While LE models tend to agree well with experimental results, TE models are known to agree less favourably. A number of reasons are known to contribute to this. First, the wavenumber frequency spectra of the wall pressure fluctuations are very sensitive to the realistic geometry and angle of attack of the aerofoils used in the TE experiments, and consequently cannot be characterized as accurately as the incoming grid turbulence in the LE noise experiments. This results in less accurate TE noise predictions. Second, when a turbulent boundary layer convects past the trailing edge of an aerofoil, noise due to other sources coexists with TE noise, such as the noise from vortex pairs and jet flows across the serration valleys [38, 39]. These additional source mechanisms lead to scattered experimental results and hence inevitable discrepancies between the experimental data and TE noise predictions.

Figure 11(a) shows the noise reduction spectra from three different experiments and one Direct Numerical Simulations (DNS). The three experiments are specifically chosen to have similar operating conditions. For example, in the experiment of León et al. [38] $M = 0.1$, $h = 1$ and the angle of attack is fixed at

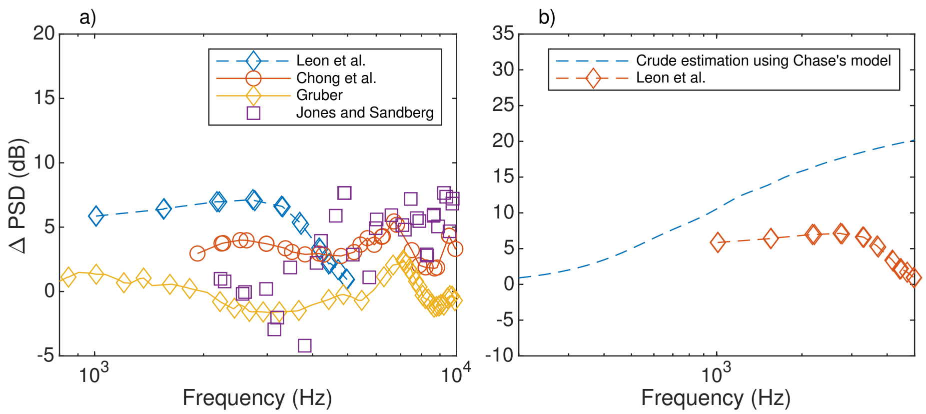

Figure 11: Noise reduction spectra due to the use of sawtooth serrations: a) experimentally measured noise reduction spectra under similar configurations are scattered across a wide range of values. In León et al. [38], $M = 0.1$, $h = 1$ and the angle of attack (AoA) is $0°$; in Chong et al. [16], $M = 0.16$, $h = 1.18$ and the AoA is $4.2°$; in Gruber [39], $M = 0.12$, $h = 0.85$ and the AoA is $5°$; in Jones and Sandberg [22], $M = 0.4$, $h = 1.2$, and the AoA is $5°$. b) a crude estimation of the TE noise reduction using Chase's model qualitatively captures the spectral trend shown in León et al. [38] at low frequencies, while deviation occurs at high frequencies mostly likely due to the appearance of other source mechanisms.

$0°$, while in the study of Chong et al. [16] $M = 0.16$, $h = 1.18$ and the angle of attack is fixed at $4.2°$. All three experiments also share similar Reynolds numbers and the serrations used in these experiments are of similar physical sizes. However, one can see that the noise reduction spectra differ significantly from each other. The sensitivity of the wall pressure fluctuations on the geometry and angle of attack of the aerofoils and the appearance of other noise source mechanisms are likely to be the primary reasons for such differences.

The aim of this section is to validate the mathematical techniques used in Section 2 to develop the rapid LE and TE models. As far as this aim is concerned, the successful validation of LE noise model in the preceding section is sufficient because of the similar mathematical techniques used in deriving both models. Nevertheless, for completeness, we can also show a brief comparison between the TE model prediction and experiment data in the literature. However, in most experiments, such as those shown in figure 11(a), the wavenumber frequency spectra of the wall pressure fluctuations beneath the turbulent boundary layers are not known. To enable a qualitative comparison, we will use Chase's model for the wall pressure spectra over flat plates to obtain a crude estimation of the noise reduction. Noting the inevitable discrepancies introduced by the use of Chase's model and the appearance of other noise source mechanisms, we do not aim for a quantitative comparison between the model predictions and the experiments, but rather our focus is on the qualitative behaviour of the estimated noise reduction and what might be educed about the complex flow behaviour in the vicinity of serrations.

Figure 11(b) shows the noise reduction spectra measured by León et al. [38] and estimated by using Chase's model and equation 21. The result of León et al. [38] is chosen because of its zero angle of attack in the experiment. In evaluating equation 21, the Mach number is taken to be $M = 0.1$, the dimensionless half root-to-tip amplitude $h = 1$, and the dimensional serration wavelength and boundary thickness are taken to be 20 mm and 15.9 mm, respectively. As can be seen from figure 11(b), at low frequencies the predicted noise reduction amplitude is close to that observed, however, as frequency increases the predicted noise reduction is increasingly large, whereas the observed reduction goes down. Such a deviation is likely to be caused by a combination of the inaccurate model for the wall pressure fluctuations and the appearance of other noise sources. In particular, the relative sharp performance drop at 3 kHz strongly suggests the emergence of other noise sources. Figure 11(b) shows the crucial importance of correctly modelling the wavenumber frequency spectra of the wall pressure fluctuations in order to correctly reproduce the experimental results. This will be studied more closely in our future work. We note that the TE model, i.e. equation 21, does not depend on any specific wall pressure spectra, and making use of spectra from either numerical simulations or experiments is very straightforward due to the remarkably simple nature of equation 21.

5. Conclusion and future work

This paper develops rapid noise prediction models for serrated leading and trailing edges. This is based on the fact that high order modes are cut-off and adjacent modes do not interfere in the far field except at sufficiently high frequencies, so the infinite-interval integral involving two infinite sums may be replaced by just one straightforward sum. The resulting models take particularly concise forms when the serration is sufficiently narrow such that the convective acoustic wavenumber $\bar{k} < \pi$ (or more roughly $\bar{k} < 2\pi$) is satisfied in the frequency range of interest. In practice this condition may afford further relaxation. A comparison of these simplified models to the full analytical solutions shows that the obtained models serve as excellent approximations over the entire frequency range of interest.

The leading-edge noise model is compared with experimental results for sawtooth serrations of various root-to-tip amplitudes. Good agreement is achieved for both $h = 1/4$ and $h = 1/2$. Deviation occurs for $h = 1$ but this is due to the contribution of trailing-edge noise to the total noise observed in the experiment, and the simplified model continues to approximate the full solution with a great degree of accuracy. Because of the lack of accurate wall pressure statistics, a qualitative TE noise estimation using Chase's model is compared with one of TE noise results measured experimentally. The results demonstrate the importance of accurately modelling the wavenumber frequency spectra for the wall pressure fluctuations beneath turbulent boundary layers in order to correctly predict TE noise.

The models developed in this paper are robust, efficient, and can be easily implemented. For example, a typical noise spectrum can be obtained within a few milliseconds using these models, while it takes hours to evaluate the original full solutions. The efficiency and robustness would allow parametric optimization studies to be performed quickly, which is important at the design stage of many applications.

Acknowledgement

The authors wish to gratefully acknowledge the financial support provided by the EPSRC under the grant number EP/P015980/1.

References

[1] R. K. Amiet, Acoustic radiation from an airfoil in a turbulent stream, Journal of Sound and Vibration 41 (1975) 407–420.

[2] T. F. Brooks, D. S. Pope, M. A. Marcolini, Airfoil self-noise and prediction, NASA reference publication (1989). NASA-RP-1218.

[3] M. S. Howe, A review of the theory of trailing edge noise, Journal of Sound and Vibration 61 (1978) 437–465.

[4] J. M. R. Graham, Similarity rules for thin aerofoils in non-stationary subsonic flows, Journal of Fluid Mechanics 43 (1970) 753–766.

[5] D. M. Bushnell, K. J. Moore, Drag reduction in nature, Annual Review of Fluid Mechanics 23 (1991) 65–79.

[6] F. E. Fish, L. E. Howle, M. M. Murray, Hydrodynamic flow control in marine mammals, Integrative and Comparative Biology 48 (2008) 788–800.

[7] H. T. C. Pedro, M. H. Kobayashi, Numerical study of stall delay on humpback whale flippers, in: Proceedings of the 46th AIAA Aerospace Sciences Meeting and Exhibit, American Institute of Aeronautics and Astonautics, 2008. AIAA 2008-584.

[8] K. Hansen, C. Doolan, R. M. Kelso, Reduction of flow induced airfoil tonal noise using leading edge sinusoidal modifications, Acoustics Australia 40 (2012) 172–177.

[9] S. Narayanan, P. Chaitanya, S. Haeri, P. Joseph, J. W. Kim, C. Polacsek, Airfoil noise reductions through leading edges serrations, Physics of Fluids 27 (025109) (2015).

[10] A. S. H. Lau, S. Haeri, J. W. Kim, The effect of wavy leading edges on aerofoil-gust interaction noise, Journal of Sound and Vibration 332 (2013) 6234–6253.

[11] J. W. Kim, S. Haeri, P. F. Joseph, On the reduction of aerofoil-turbulence interaction noise associated with wavy leading edges, Journal of Fluid Mechanics 792 (2016) 526–552.

[12] J. M. Turner, J. W. Kim, Towards understanding aerofoils with dual-frequency wavy leading edges interacting with vortical distrubances, in: Proceedings of the 22nd AIAA/CEAS Aeroacoustics Conference, American Institute of Aeronautics and Astronautics, 2016. AIAA 2016-2951.

[13] B. Lyu, M. Azarpeyvand, On the noise prediction for serrated leading edges, Journal of Fluid Mechanics 826 (2017) 205–234.

[14] L. J. Ayton, P. Chaitanya, An analytical and experimental investigation of aerofoil-turbulence interaction noise for plates with spanwise-varying leading edges, Journal of Fluid Mechanics 865 (2019) 137–168.

[15] A. G. M. Dassen, R. Parchen, J. Bruggeman, F. Hagg, Results of a wind tunnel study on the reduction of airfoil self-noise by the application of serrated blade trailing edges, Proceeding of the European Union Wind Energy Conference and Exhibition (1996) 800–803.

[16] T. P. Chong, P. F. Joseph, M. Gruber, Airfoil self noise reduction by non-flat plate type trailing edge serrations, Applied Acoustics 74 (2013) 607–613.

[17] D. J. Moreau, C. J. Doolan, Noise-reduction mechanism of a flat-plate serrated trailing edge, AIAA Journal 51 (2013) 2513–2522.

[18] S. Oerlemans, M. Fisher, T. Maeder, K. Kögler, Reduction of wind turbine noise using optimized airfoils and trailing-edge serrations, AIAA Journal 47 (2009) 1470–1481.

[19] M. Gruber, P. F. Joseph, M. Azarpeyvand, An experimental investigation of novel trailing edge geometries on airfoil trailing edge noise reduction, in: Proceedings of 19th AIAA/CEAS Aeroacoustics Conference, Aeroacoustics Conferences, American Institute of Aeronautics and Astronautics, 2013. AIAA 2013-2011.

[20] T. P. Chong, A. Vathylakis, On the aeroacoustic and flow structures developed on a flat plate with a serrated sawtooth trailing edge, Journal of Sound and Vibration 354 (2015) 65–90.

[21] C. A. Leon, R. Merino-Martinez, D. Ragni, F. Avallone, F. Scarano, S. Probsting, M. Snellen, D. G. Simons, J. Madsen, Effect of trailing edge serration-flow misalignment on airfoil noise emissions, Journal of Sound and Vibration 406 (2016) 19–33.

[22] L. E. Jones, R. D. Sandberg, Acoustic and hydrodynamic analysis of the flow around an aerofoil with trailing-edge serrations, Journal of Fluid Mechanics 706 (2012) 295–322.

[23] M. Sanjosé, C. Meon, V. Masson, S. Moreau, Direct numerical simulation of acoustic reduction using serrated trailing-edge on an isolated airfoil, in: Proceedings of the 20th AIAA/CEAS Aeroacoustics Conference, American Institute of Aeronautics and Astronautics, 2014. AIAA 2014-2324.

[24] W. C. van der Velden, F. Avallone, D. Ragni, Numerical analysis of noise reduction mechanisms of serrated trailing edges under zero lift conditions, in: Proceedings of the 23rd AIAA/CEAS Aeroacoustics Conference, American Institute of Aeronautics and Astronautics, 2017. AIAA 2017-4173.

[25] M. S. Howe, Aerodynamic noise of a serrated trailing edge, Journal of Fluids and Structures 5 (1991) 33–45.

[26] M. S. Howe, Noise produced by a sawtooth trailing edge, The Journal of the Acoustical Society of America 90 (1991) 482–487.

[27] M. Azarpeyvand, M. Gruber, P. F. Joseph, An analytical investigation of trailing edge noise reduction using novel serrations, in: Proceedings of 19th AIAA/CEAS Aeroacoustics Conference, Aeroacoustics Conferences, 2013. AIAA 2013-2009.

[28] B. Lyu, M. Azarpeyvand, S. Sinayoko, Noise prediction for serrated trailing edges, Journal of Fluid Mechanics 793 (2016) 556–588.

[29] B. Lyu, M. Azarpeyvand, S. Sinayoko, A trailing-edge noise model for serrated edges, in: Proceeding of 21st AIAA/CEAS Aeroacoustics Conference, Aeroacoustics Conferences, American Institute of Aeronautics and Astronautics, 2015. AIAA 2015-2362.

[30] R. K. Amiet, Noise due to turbulent flow past a trailing edge, Journal of Sound and Vibration 47 (1976) 387–393.

[31] S. Sinayoko, M. Azarpeyvand, B. Lyu, Trailing edge noise prediction for rotating serrated blades, in: Proceeding of 20th AIAA/CEAS Aeroacoustics Conference, Aeroacoustics Conferences, American Institute of Aeronautics and Astronautics, 2014. AIAA 2014-3296.

[32] L. J. Ayton, Analytical solution for aerodynamic noise generated by plates with spanwise-varying trailing edges, Journal of Fluid Mechanics 849 (2018) 448–466.

[33] M. Roger, S. Moreau, Back-scattering correction and further extensions of Amiet's trailing-edge noise model. part 1: theory, Journal of Sound and Vibration 286 (2005) 477–506.

[34] B. Lyu, L. J. Ayton, P. Chaitanyan, Acoustic optimality of leading-edge serration profiles, Journal of Sound and Vibration 462 (114923) (2019).

[35] B. Lyu, M. Azarpeyvand, S. Sinayoko, Noise prediction for serrated leading-edges, in: Proceeding of 22nd AIAA/CEAS Aeroacoustics Conference, Aeroacoustics Conferences, American Institute of Aeronautics and Astronautics, 2016. AIAA 2016-2740.

[36] D. M. Chase, The character of the turbulent wall pressure spectrum at subconvective wavenumbers and a suggested comprehensive model, Journal of Sound and Vibration 112 (1987) 125–147.

[37] G. Bampanis, M. Roger, D. Ragni, F. Avallone, C. Teruna, Airfoil-turbulence interaction noise source identification and reduction by leading-edge serrations, in: Proceedings of 25th AIAA/CEAS Aeroacoustics Conference, Aeroacoustics Conferences, American Institute of Aeronautics and Astronautics, 2019. AIAA 2019-2741.

[38] C. A. León, D. Ragni, S. Pr obsting, F. Scarano, J. Madsen, Flow topology and acoustic emissions of trailing edge serrations at incidence, Experiments in Fluids 57 (91) (2016).

[39] M. Gruber, Airfoil noise reduction by edge treatments, Ph.D. thesis, University of Southampton, University Road, Southampton SO17, 1BJ, 2012.